Normal and Frictional Forces between Surfaces Bearing Polyelectrolyte Brushes

Uri Raviv,*[,†,‡] Suzanne Giasson,*[,§,||] Nir Kampf,[†] Jean-François Gohy,[⊥,#] Robert Jérôme,[⊥] and Jacob Klein*[,†,▽]

Department of Materials and Interfaces, Weizmann Institute of Science, Rehovot 76100, Israel, Physical and Theoretical Chemistry Laboratory, Oxford University, South Parks Road, Oxford OX1 3QZ, U.K., Department of Chemical Engineering and CERSIM, Laval University, Québec, Canada, G1K 7P4, and Center for Education and Research on Macromolecules, University of Liège, Sart-Tilman B6, 4000 Liège, Belgium

Received December 19, 2007

Normal and shear forces were measured as a function of surface separation, D, between hydrophobized mica surfaces bearing layers of a hydrophobic−polyelectrolytic diblock copolymer, poly(methyl methacrylate)-*block*-poly(sodium sulfonated glycidyl methacrylate) copolymer (PMMA-*b*-PSGMA). The copolymers were attached to each hydrophobized surface by their hydrophobic PMMA moieties with the nonadsorbing polyelectrolytic PSGMA tails extending into the aqueous medium to form a polyelectrolyte brush. Following overnight incubation in 10^{-4} w/v aqueous solution of the copolymer, the strong hydrophobic attraction between the hydrophobized mica surfaces across water was replaced by strongly repulsive normal forces between them. These were attributed to the osmotic repulsion arising from the confined counterions at long-range, together with steric repulsion between the compressed brush layers at shorter range. The corresponding shear forces on sliding the surfaces were extremely low and below our detection limit (±20−30 nN), even when compressed down to a volume fraction close to unity. On further compression, very weak shear forces (130 ± 30 nN) were measured due to the increase in the effective viscous drag experienced by the compressed, sliding layers. At separations corresponding to pressures of a few atmospheres, the shearing motion led to abrupt removal of most of the chains out of the gap, and the surfaces jumped into adhesive contact. The extremely low frictional forces between the charged brushes (prior to their removal) is attributed to the exceptional resistance to mutual interpenetration displayed by the compressed, counterion-swollen brushes, together with the fluidity of the hydration layers surrounding the charged, rubbing polymer segments.

Introduction

Polyelectrolytes at surfaces play an important role in colloid stabilization by controlling the interactions through a combination of electrostatic and steric interactions.[1] Several experimental[2–15] and theoretical[1,16–27] studies have explored the intrinsic structure and properties of polyelectrolyte brushes as a function of grafting density, charge density, and ionic strength. Those studies established that charged brushes may be stretched more strongly than the equivalent neutral brushes in a good solvent at corresponding densities. The normal forces between two opposing surfaces bearing grafted polyelectrolytes have also been investigated.[1,6–8,21,28,29] It has been found that the repulsive forces between grafted polyelectrolytes, unlike neutral brushes, may at low salt concentration commence at separations much larger than the range of steric repulsion, due to long-ranged double-layer electrostatic interactions. In addition, once brush overlap occurs, the magnitude of the interaction may exceed that of the corresponding neutral chains, due to the additional osmotic pressure of the counterions. With increasing salt concentration polyelectrolyte brushes collapse but only as a relatively weak power law of the salt concentration.[1,6,8,22,29] This collapse may increase the viscosity of the layers and influence their frictional behavior.[30]

* To whom correspondence should be addressed. E-mail: jacob.klein@weizmann.ac.il (J.K.), or suzanne.giasson@umontreal.ca (S.G.), or raviv@chem.ch.huji.ac.il (U.R.).

[†] Weizmann Institute of Science.

[‡] Present address: The Chemistry Institute, The Hebrew University of Jerusalem, Givat Ram, 91904, Jerusalem, Israel.

[§] Laval University.

[||] Present address: Département de Chimie et Faculté de Pharmacie, Université de Montréal, C.P. 6128, succ. Centre-Ville, Montréal, Québec, Canada H3C 3J7.

[⊥] University of Liège.

[#] Present address: Unité de Chimie des Matériux Inorganiques et Organiques (CMAT), Département de Chimie, Université catholique de Louvain, Place L. Pasteur 1, B-1348 Louvain-la-Neuve, Belgium.

[▽] Oxford University.

(1) Pincus, P. *Macromolecules* **1991**, *24*, 2912–2919.
(2) Muller, F.; Fontaine, P.; Delsanti, M.; Belloni, L.; Yang, J.; Chen, Y. J.; Mays, J. M.; Lesieur, P.; Tirrell, M.; Guenoun, P. *Euro. Phys. J. E* **2001**, *6*, 109–115.
(3) Abraham, T.; Giasson, S.; Gohy, J. F.; Jerome, R.; Stamm, M. *Macromolecules* **2000**, *33*, 6051–6059.
(4) Mir, Y.; Auroy, P.; Auvray, L. *Phys. Rev. Lett.* **1995**, *75*, 2863–2866.
(5) Zhang, Y.; Tirrell, M.; Mays, J. W. *Macromolecules* **1996**, *29*, 7299–7301.
(6) Balastre, M.; Li, F.; Schorr, P.; Yang, J.; Mays, J. W.; Tirrell, M. *Macromolecules* **2002**, *33*, 9480–9486.
(7) Tirrell, M. *J. Colloid Interface Sci.* **1997**, *2*, 70–75.
(8) Tamashiro, M. N.; Hernandez-Zapata, E.; Schorr, P. A.; Balastre, M.; Tirrell, M.; Pincus, P. *J. Chem. Phys.* **2001**, *115*, 1960–1969.
(9) Guenoun, P.; Muller, F.; Delsanti, M.; Auvray, L.; Chen, Y. J.; Mays, J. W.; Tirrell, M. *Phys. Rev. Lett.* **1998**, *81*, 3872–3875.
(10) Ahrens, H.; Forster, S.; Helm, C. A. *Phys. Rev. Lett.* **1998**, *81*, 4172–4175.
(11) An, S. W.; Thirtle, P. N.; Thomas, R. K.; Baines, F. L.; Billingham, N. C.; Armes, S. P.; Penfold, J. *Macromolecules* **1999**, *32*, 2731–2738.
(12) Tran, Y.; Auroy, P.; Lee, L. T. *Macromolecules* **1999**, *32*, 8952–8964.
(13) Kampf, N.; Gohy, J. F.; Jerome, R.; Klein, J. *J. Polym. Sci. B-Polym. Phys.* **2005**, *43*, 193–204.
(14) Yan, X.; Perry, S.; Spencer, N.; Pasche, S.; De Paul, S.; Textor, M.; Lim, M. *Langmuir* **2004**, *20*, 423–428.
(15) Muller, M.; Lee, S.; Spikes, H.; Spencer, N. *Tribol. Lett.* **2003**, *15*, 395–405.
(16) Miklavic, S. J.; Marcelja, S. *Macromolecules* **1988**, *92*, 6718–6722.
(17) Argillier, J. F.; Tirrell, M. *Theor. Chim. Acta* **1992**, *82*, 343–350.
(18) Borisov, O. V.; Zhulina, E. B.; Birshtein, T. M. *Macromolecules* **1994**, *27*, 4795–4803.
(19) Misra, S.; Tirrell, M.; Mattice, W. *Macromolecules* **1996**, *29*, 6056–6060.

10.1021/la7039724 CCC: $40.75
Published on Web 07/19/2008

More recently, surface force balance (SFB) investigations, where forces between bare or polymer-bearing mica surfaces are measured directly as a function of their separation, have been extended to the case of lateral interactions, that is, the forces that act between surfaces as they slide past each other, while mutually compressed. There is a marked contrast in the shear and frictional behavior of polymer-coated surfaces relative to bare surfaces across monomeric liquids. Simple nonassociating liquids may exhibit a yield point or critical shear stress and their effective viscosity diverges by several orders of magnitude when confined (even at low or zero pressure) to films 5−8 monolayers thick or less.[31–36] The case of essentially salt-free (so-called conductivity) water and of dilute salt solutions is different: these retain a fluidity close to their bulk value at film thicknesses down to within 1−2 monolayers at most.[37–42] More concentrated salt solution can result in hydrated ions trapped between charged surfaces,[38,43–47] leading to low frictional forces as the surfaces slide past each other at pressures up to several atmospheres;[38] at very high loads, however, surface damage may occur.[38,48,49] The attachment of polymers to the surfaces, on the other hand, may greatly reduce their sensitivity to damage by providing a steric barrier against adhesion during shear and provides very efficient lubrication in a good solvent, up to moderate compressions.

The modification of shear or frictional forces by neutral adsorbed[50,51] and end-grafted polymers[52–56] has been investigated in nonpolar solvents. The forces depend on the interactions between the polymer and the sliding surfaces as well as on solvent quality.[51,53,57] Polystyrene brushes on mica substrates across a good solvent have been shown to provide excellent lubrication due to weak interpenetration of the opposing layers and a consequent fluid interfacial layer, up to moderate compressions (mean pressure across the contact area of order 5 atm). At higher pressures, the polymer approaches its glassy concentration, the shear forces rise sharply. and the interfacial sliding reverts from the midplane—halfway between the brush-bearing surfaces—to the underlying substrate.[54,58] For low glass transition temperature brushes,[59] the frictional drag at high compression can be well-understood in terms of stretching and disentangling of the opposing chains as the compressed brush-coated surfaces slide past each other. Similar sliding effects are observed with adsorbed polyethylene oxide chains across a good solvent when sliding at high pressures.[50]

Shear forces between mutually compressed surfaces bearing adsorbed[60] and grafted[61] polyelectrolytes have been recently studied. Sheared polyelectrolyte chains are often found in living systems, such as between the eyelid and the cornea, between cells transporting on the extracellular matrix, and in biolubrication.[62–65] The extra repulsion provided by the osmotic pressure of the free counterions associated with the chains may significantly influence the lateral interactions between polyelectrolyte layers. In this paper, we extend our earlier brief report[61] and investigate the normal and particularly the *shear* forces between polyelectrolyte brushes immersed in an aqueous medium. More specifically, we report on several additional control experiments, the normal forces after shearing the modified surfaces, the refractive index of the confined films (from which we were able to estimate the polymer absorbance), and a more detailed analysis of our data. Our study confirms the long-ranged repulsive forces between polyelectrolyte brushes[3,29] and reveals that the frictional forces between the compressed charged brushes are remarkably low at pressures approaching physiologically relevant ones.

Materials and Methods

Materials. Ultrapure (conductivity) water was obtained as described elsewhere.[66] The ethanol and toluene (analytical grade A.R.) used for the cleaning procedure were supplied by Bio-Laboratory Inc. The 30% H_2O_2 solution was supplied by Frutarom Ltd., and the 95−97% H_2SO_4 A.R. solution was supplied by Palacid Ltd. The mica was ruby muscovite, grade 1, supplied by S & J Trading Inc. An epoxy, EPON 1004 resin (Shell), was used to glue the mica sheets to the cylindrical quartz lenses.

(20) Pryamitsyn, V. A.; Leermakers, F. A. M.; Fleer, J.; Zhulina, E. B. *Macromolecules* **1996**, *29*, 8260–8270.
(21) Zhulina, E. B.; Borisov, O. V. *J. Chem. Phys.* **1997**, *107*, 5952–5967.
(22) Zhulina, E. B.; Wolterink, J. K.; Borisov, O. V. *Macromolecules* **2000**, *33*, 4945–4953.
(23) Dobrynin, A. V.; Rubinstein, M. *Prog. Polym. Sci.* **2005**, *30*, 1049–1118.
(24) Dobrynin, A. V.; Rubinstein, M. *Macromolecules* **2002**, *35*, 2754–2768.
(25) Dobrynin, A. V.; Deshkovski, A.; Rubinstein, M. *Macromolecules* **2001**, *34*, 3421–3436.
(26) Dobrynin, A. V.; Deshkovski, A.; Rubinstein, M. *Phys. Rev. Lett.* **2000**, *84*, 3101–3104.
(27) Dobrynin, A. V.; Colby, R. H.; Rubinstein, M. *Macromolecules* **1995**, *28*, 1859–1871.
(28) Liberelle, B.; Giasson, S. *Langmuir* **2008**, *24*, 1550–1559.
(29) Abraham, T.; Giasson, S.; Gohy, J. F.; Jerome, R. *Langmuir* **2000**, *16*, 4286–4292.
(30) Gelbert, M.; Biesalski, M.; Ruhe, J.; Johannsmann, D. *Langmuir* **2000**, *16*, 5774–5784.
(31) Gao, J.; Luedtke, W. D.; Landman, U. *J. Phys. Chem. B* **1997**, *101*, 4013–4023.
(32) Chan, D. Y. C.; Horn, R. G. *J. Chem. Phys.* **1985**, *83*, 5311–5324.
(33) Klein, J.; Kumacheva, E. *Science* **1995**, *269*, 816–819.
(34) Klein, J.; Kumacheva, E. *J. Chem. Phys.* **1998**, *108*, 6996–7009.
(35) Kumacheva, E.; Klein, J. *J. Chem. Phys.* **1998**, *108*, 7010–7022.
(36) Israelachvili, J. N.; McGuiggan, P. M. *Science* **1988**, *240*, 189–191.
(37) Raviv, U.; Laurat, P.; Klein, J. *Nature* **2001**, *413*, 51–54.
(38) Raviv, U.; Klein, J. *Science* **2002**, *297*, 1540–1543.
(39) Raviv, U.; Kampf, N.; Klein, J. In *Dynamics and Friction at Submicrometer Confining Systems*; Braiman, Y.; Drake, M.; Family, F.; Klafter, J., Eds.; ACS Symposium Series; American Chemical Society: Washington, DC, 2004; pp 131−138.
(40) Raviv, U.; Giasson, S.; Frey, J.; Klein, J. *J. Phys. Condens. Matter* **2002**, *14*, 9275–9283.
(41) Raviv, U.; Perkin, S.; Laurat, P.; Klein, J. *Langmuir* **2004**, *20*, 5322–5332.
(42) Perkin, S.; Chai, L.; Kampf, N.; Raviv, U.; Briscoe, W.; Dunlop, I.; Titmuss, S.; Seo, M.; Kumacheva, E.; Klein, J. *Langmuir* **2006**, *22*, 6142–6152.
(43) LeNeveu, D. M.; Rand, R. P.; Parsegian, V. A. *Nature* **1976**, *259*, 601.
(44) Israelachvili, J. N.; Adams, G. E. *J. Chem. Soc. Faraday Trans. 1* **1978**, *79*, 975–1001.
(45) Pashley, R. M. *J. Colloid Interface Sci.* **1981**, *80*, 153–162.
(46) Pashley, R. M. *J. Colloid Interface Sci.* **1981**, *83*, 531–546.
(47) Pashley, R. M.; Israelachvili, J. N. *J. Colloid Interface Sci.* **1984**, *101*, 511–523.
(48) Homola, A. M.; Israelachvili, J. N.; Mcguiggan, P. M.; Gee, M. L. *Wear* **1990**, *136*, 65–83.
(49) McGuiggan, P. M.; Pashley, R. M. *J. Phys. Chem.* **1988**, *92*, 1235–1239.
(50) Raviv, U.; Tadmor, R.; Klein, J. *J. Phys. Chem. B* **2001**, *105*, 8125–8134.
(51) Klein, J.; Kumacheva, E.; Perahia, D.; Mahalu, D.; Warburg, S. *Faraday Discuss.* **1994**, *98*, 173–188.
(52) Klein, J.; Kumacheva, E.; Mahalu, D.; Perahia, D.; Fetters, L. *Nature* **1994**, *370*, 634–636.
(53) Klein, J. *Annu. Rev. Mater. Sci.* **1996**, *26*, 581–612.
(54) Klein, J.; Kumacheva, E.; Perahia, D.; Fetters, L. J. *Acta Polym.* **1998**, *49*, 617–625.
(55) Schorr, P.; Kwan, T.; Kilbey, M.; Shaqfeh, S. G.; Tirrell, M. *Macromolecules* **2003**, *36*, 389–398.
(56) Schorr, P.; Kilbey, S. M.; Tirrell, M. *Polym. Prepr. (Abstr. Am. Chem. Soc.)* **1999**, *218*(278-POLY, Part 2 AUG), U477.
(57) Subbotin, A.; Semenov, A.; Hadziioannou, G.; ten Brinke, G. *Macromolecules* **1995**, *28*, 1511.
(58) Klein, J., In *Fundamentals of Tribology and Bridging the Gap between the Macro- and Micro/Nanoscale*; Bhushan, B., Ed.; Kluwer Academic Publishers: The Netherlands, 2001; 177.
(59) Tadmor, R.; Janik, J.; Fetters, L. J.; Klein, J. *Phys. Rev. Lett.* **2003**, *91*, 115503.
(60) Kampf, N.; Raviv, U.; Klein, J. *Macromolecules* **2004**, *37*, 1134–1142.
(61) Raviv, U.; Giasson, S.; Kampf, N.; Gohy, J. F.; Jerome, R.; Klein, J. *Nature* **2003**, *425*, 163–165.
(62) *Proc. Inst. Mech. Eng. Part H: Eng. Med.*, **1987**, *210* (Special Issue on Biolubrication).
(63) Dowson, D.; Wright, V., Biolubrication review paper. In *Bio-tribology*; Institute of Petroleum: London, 1973; pp 81−88..
(64) Jin, M. S.; Grodzinsky, A. J. *Macromolecules* **2001**, *34*, 8330–8339.
(65) Klein, J. *Proc. Inst. Mech. Eng. Part J: J. Eng. Tribol.* **2006**, *220*, 691−710.
(66) Raviv, U.; Frey, J.; Sak, R.; Laurat, P.; Tadmor, R.; Klein, J. *Langmuir* **2002**, *18*, 7482–7495.

Table 1. Molecular Characteristics of the Polymers Used

polymer	N^a	M_n	M_w/M_n	$N_s{}^b$
PMMA block	$N_1 = 41$	4 100	1.05	0
PSGMA block	$N_2 = 115$	24 700	1.1	80
PMMA-*b*-PSGMA diblock copolymer	156	28 800		80
PSGMA homopolymer	47	10 000	1.8	33

[a] Number of monomers. [b] Number of monomers with sulfonate group.

Stearic trimethylammonium iodide (STAI: $CH_3(CH_2)_{17}N^+(CH_3)_3I^-$) was synthesized according to known methods.[67,68] Poly(methyl methacrylate)-*block*-poly(sodium sulfonated glycidyl methacrylate) copolymer, PMMA-*b*-PSGMA, and PSGMA polymer were anionically synthesized and characterized as reported in detail elsewhere.[29,69,70] The copolymer is a hydrophobic (PMMA)−hydrophilic (polyelectrolytic) (PSGMA) diblock: $(CH_2C(CH_3)CO_2CH_3)_{N_1}(CH_2C(CH_3)CO_2CH_2CHOHCH_2SO_3^-Na^+)_{N_2}$. The copolymer was analyzed by size exclusion chromatography (SEC) and proton nuclear magnetic resonance (^{1}H NMR), and its molecular characteristic features are summarized in Table 1.[70] The degree of sulfonation, $\varphi = 70\%$, was determined by titration. The charge of the copolymer is independent of the local pH because the ionizable groups are sulfonate groups (SO_3^-), which are strong acids. The copolymer was deoxygenated and purified by dialysis against regularly replaced distilled water (Spectra-Por membranes, cutoff 10 000 Da). The PMMA-*b*-PSGMA molecule behaves as a self-associating macrosurfactant with a critical micelle concentration (cmc) of ca. 1.0 ± 0.2 mg/mL as determined by surface tension measurement and dynamic light scattering measurements.[70] Our solutions were far below this concentration. The molecular characteristics of PSGMA (Table 1) were determined from aqueous GPC calibrated with poly(styrene sulfonate) standards.

Methods. *Surface Forces Balance.* The surface forces technique and detailed experimental procedures used to measure the normal and shear forces have been well-described elsewhere.[34,66,71] However, some experimental details are worth mentioning. Two half-silvered mica sheets are mounted face-to-face on two cylindrical lenses in a crossed-cylinder configuration. A white-light multiple-beam interferometry technique is used to measure the closest distance D between the two surfaces within an accuracy of ±0.2−0.3 nm as well as the mean curvature radius R of the surfaces. The lower surface is mounted onto a horizontal stainless steel leaf spring (spring constant $k_n = 150$ N/m) and its bending, ΔD, is measured via the interferometry technique to determine the normal force $F_n(D) = k_n\Delta D$. The upper surface mount is coupled to a four-sectored piezoelectric tube (PZT), supplied by Ferroperm (Pz29). By applying suitable potentials to opposite sectors, lateral motion $\Delta x_0(t)$ is obtained with respect to the lower surface. Shear forces between the surfaces $F_s(D)$ are transmitted to vertical springs ($k_s = 300$ N/m), whose bending as a function of time $\Delta x(t)$ is measured, via an air-gap capacitor, and yields the shear forces $F_s(D,t) = k_s\Delta x(t)$. (A schematic of the SFB is given at the inset to Figure S1 of the Supporting Information). The cleaning procedure used and the way the liquids were introduced into the SFB are described elsewhere[66] and in the Supporting Information. Measurements were carried out at 23 ± 1 °C.

The noise level in the shear measurements $\delta F_s(D)$ prior to processing is optimally ±0.1 μN[34] but somewhat worse in the present experiments, where it is ±0.5−1.0 μN, due to ambient vibrations that are transmitted despite the electronic vibration isolation system. To extract a lower signal level, a Fourier transform of the shear traces was performed and the amplitude at the applied frequency was evaluated. The sensitivity in measuring the shear forces, following subtraction of the systematic contribution of the PZT wires (ca. 100 nN) at large separations and Fourier analysis,[66] is better than ±30 nN.

The normal force profiles $F_n(D)$ vs D from different experiments, measured during the approach and separation of the surfaces, are shown with the force axis normalized as $F_n(D)/R$. Within the Derjaguin approximation[72] (for $R \gg D$), $F_n(D)/2\pi R$ is the corresponding energy per unit area, $E(D)$, for two flat parallel surfaces a distance D apart obeying the same force−distance law, making it possible to compare $F_n(D)/R$ from different experiments.

Hydrophobizing Mica Surfaces. In order to attach the PMMA-*b*-PGMAS, the mica surfaces were first hydrophobized with STAI as described and characterized in earlier studies.[40,68] Advancing contact angles (see Supporting Information) of water on such hydrophobized mica surfaces were measured. The initial contact angle (immediately after depositing the surfactant layer) was about 85° and reached 82° after 5 days of immersion in conductivity water. This is in agreement with an earlier report[68] and suggests that the STAI forms a collapsed hydrophobic layer on the surface following adsorption from aqueous solution and rinsing in conductivity water and is moreover stable for at least 5 days.

Results

Control Measurements. Detailed description of the controls is given in the Supporting Information. Briefly, the wavelength of the interference fringes at air contact separation was established, after mounting the mica surfaces into the SFB. The surfaces were then separated (∼2 mm apart) and the SFB's cell was filled with conductivity water, to ensure the removal of the water-soluble layer (mainly CO_2 and vapor[73]) and to establish the reference distance $D = D_0 = 0.0 \pm 0.3$ nm, which was at position −0.4 ± 0.3 nm, with respect to air contact. After allowing 1 h for thermal equilibration, measurements of normal force profiles were performed and revealed the long-ranged repulsion due to counterion osmotic pressure, followed by a jump, on approach, into adhesive contact, in agreement with earlier studies,[37,39–41,45,74,75] as shown in Figure S1 of the Supporting Information. Then PMMA-*b*-PSGMA was added, to control for its nonadsorbance on bare mica, and following 12 h incubation in the solution (with surfaces kept far apart) force profiles were again measured and the data, which indicate essentially no adsorption of PMMA-*b*-PSGMA on bare mica, is shown in Figures S1 and S2 of the Supporting Information. The polymer was removed by successive dilutions with water.

The mica surfaces were then taken out of the SFB cell, hydrophobized, and mounted back into the SFB as close as possible to their original orientation and the cell was filled with conductivity water. At this point the exact original relative position of the mica surfaces is lost and a small error (ca. ±0.5 nm) in the measurement of the thickness of each monolayer may occur[68] (i.e., a systematic total uncertainty of as much as ca. 1 nm in D). Following 1 h of thermal incubation, normal force profiles were determined. The surfaces jumped, on approach, to a strongly adhesive contact due to hydrophobic attraction[76] between the STAI layers (the average force curve is shown in the inset to Figure 1 and detailed results are given in Figure S3 of the Supporting Information). In two control experiments, conductivity water was replaced by PSGMA solutions as a control to examine whether the polyelectrolyte adsorbs onto the hydrophobized mica. Normal and shear forces were measured after an incubation period of 0.5−13 h in the PSGMA solution (during which time the surfaces were kept well apart) and following replacement of the PSGMA solution by conductivity water. The results show only

(67) Kodama, M.; et al. *J. Phys. Chem.* **1990**, *94*, 815.
(68) Tadmor, R.; Rosensweig, R. E.; Frey, J.; Klein, J. *Langmuir* **2000**, *16*, 9117–9120.
(69) Leemans, L.; Fayt, R. *J. Polym. Sci.* **1990**, *28*, 1255.
(70) Gohy, J. F.; Antoun, S.; Jerome, R. *Polymer* **2001**, *42*, 8637–8645.
(71) Klein, J. *J. Chem. Soc., Faraday Trans. 1* **1983**, *79*, 99–118.
(72) Derjaguin, B. V. *Kolloid Zh.* **1934**, *69*, 155–164.
(73) Poppa, H.; Elliot, A. G. *Surf. Sci.* **1971**, *24*, 149–163.
(74) Klein, J.; Raviv, U.; Perkin, S.; Kampf, N.; Giasson, S. *J. Phys.: Condens. Matter* **2004**, *16*, S5437−S5448.
(75) Raviv, U.; Laurat, P.; Klein, J. *J. Chem. Phys.* **2002**, *116*, 5167–5172.
(76) Christenson, H. K.; Claesson, P. M. *Adv. Colloid Interface Sci.* **2001**, *91*, 391–436.

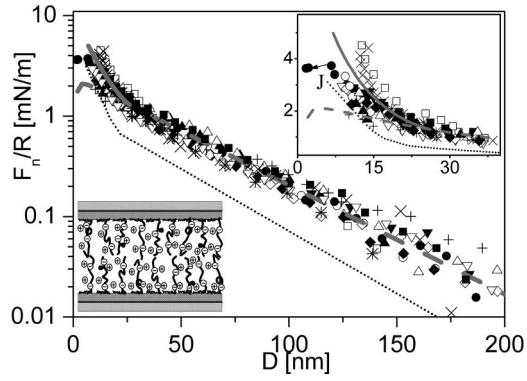

Figure 1. Normalized $F_n(D)$ profiles between STAI-coated mica surfaces prior to and following incubation to saturation in 100 ± 10 μg/mL PMMA-*b*-PSGMA aqueous solution. Solid symbols and crosses (× and +) indicate forces measured on compression and open symbols and asterisks indicate forces measured on decompression. Results from two different sets of experiments (different pairs of mica sheets) and different contact positions, measured on the first and second compression−decompression cycles, are shown. The dotted curve is the $F_n(D)$ between STAI-coated mica surfaces immersed in 70 ± 5 μg/mL PSGMA homopolymer aqueous solution and is identical to the broken line in Figure S4A of the Supporting Information. The dashed curve is a fit to a DLVO expression,[77,78] $F_n(D)/R = 128\pi ck_BT\kappa^{-1}\tanh^2(e\psi_0/4k_BT)\exp(-\kappa D) - A_H/6D^2$, where c is the ion concentration, T is the temperature, k_B is the Boltzmann constant, A_H is the Hamaker constant, ψ_0 is the effective (large-separation) surface potential, and $\kappa^{-1} = (\varepsilon k_BT/8\pi e^2c)^{1/2}$ is the Debye length, where $\varepsilon = 80.1$ is the dielectric constant of water and e is the electronic charge. We used $A_H = 1.5 \times 10^{-20}$ J, which is the maximum possible theoretical value for the interaction of two hydrocarbon-coated mica surfaces[84]). The solid curve is the expression accounting for the short-ranged repulsive forces given in eq 9, with $A = 2.8 \times 10^{-2}$, $B = 9 \times 10^{-3}$ (see ref 96) and the DLVO parameters of the long-ranged interaction. The solid circles indicate the $F_n(D)$ profile measured after shear, where it is possible to approach down to $D = 6.7 \pm 0.3$ nm, under a load of 3.7 mN/m, from which there is a jump-in to a flat contact at $D = 2.1 \pm 0.3$ nm (indicated with an arrow and J at the inset). The upper right inset shows the forces over the last 40 nm on a magnified linear scale. The lower left inset shows schematically the two STAI-coated mica surfaces with the polyelectrolyte brushes formed by the diblock copolymer chains and their associated counterions.

marginal weak adsorption of the PSGMA block onto the STAI layers (see Figure S4 of the Supporting Information).

PMMA-*b*-PSGMA on STAI. In other experiments, following the controls between STAI-coated surfaces in polymer-free water, PMMA-*b*-PSGMA solution in conductivity water was introduced into the SFB to a concentration of 100 ± 10 μg/mL, while the surfaces were kept far apart across the solution and avoiding at all times their exposure to the air−water interface. After an incubation period of 14 ± 1 h, $F_n(D)$, profiles were then measured, as shown in Figure 1. These normal interactions are consistent with a previous study carried out on a similar type of polyelectrolyte/hydrophobic moiety diblock.[29] Long-ranged repulsive forces commenced at 200 nm and increased monotonically with decreasing D. The long ranged repulsive force is well-depicted, down to $D = 20 \pm 3$ nm, by an electrostatic contribution of the DLVO theory:[77,78]

$$F_n(D)/R = 128\pi ck_BT\kappa^{-1}\tanh^2(e\psi_0/4k_BT)\exp(-\kappa D) - A_H/6D^2 \quad (1)$$

where c is the ion concentration, T is the temperature, k_B is the Boltzmann constant, A_H is the Hamaker constant, ψ_0 is the effective (large-separation) surface potential, and $\kappa^{-1} = (\varepsilon k_BT/8\pi e^2c)^{1/2}$ is the Debye length, where $\varepsilon = 80.1$ is the dielectric constant of water and e is the electronic charge. From the fit to the data we find that $\kappa^{-1} = \kappa_s^{-1} = 40 \pm 3$ nm (compared to 75 nm in pure water, see Figure S1) corresponding to $c = c_s = (6 \pm 1) \times 10^{-5}$ M and $\psi_0 = 210 \pm 50$ mV (compared with 100 mV in pure water; see the Supporting Information), corresponding to a surface charge density, σ_0, of $1e/(7 \pm 1)$ nm^2. σ_0 was calculated from the surface potential using the Grahame equation, which for 1:1 electrolyte has the form $\sigma_0 = (8k_BTc\varepsilon\varepsilon_0)^{1/2}\sinh(e\psi_0/2k_BT)$. As the effective polymer size is small compared to κ^{-1} (the contour length of the polyelectrolyte block is ca. 29 nm), the DLVO treatment is valid.[79] We note that eq 1 has been derived with the assumption that the charge density is evenly smeared on the interacting surfaces and that there is no ion penetration inside the surfaces. In the case of brushes, the volume charge density rather than surface charge density has to be considered. This changes the solution of the Poisson−Boltzmann equation for the electrostatic potential of the system and leads to a more complex expression for the interaction energy and the force.[21,80] However, this treatment is beyond the scope of this experimental paper.

The value of ψ_0 is based on the assumption that the double-layer theory applies down to D_0. As most of the mica surface charges are neutralized by the STAI, this value of ψ_0 does not correspond to the potential at zero distance, D_0. A possible way to overcome this[79] is to introduce an outer Helmholtz plane (OHP), D_h, by replacing the exponential term in eq 1, $\exp(-\kappa D)$, with $\exp[-\kappa(D - 2D_h)]$. If we consider the OHP to be located at a distance equivalent to the equilibrium thickness of the layers, L (see below), i.e., $D_h = L = 13 \pm 2$ nm, we obtain for a distance D_h from the mica surface a potential ψ of 100 ± 10 mV, corresponding to a net charge density σ of $1e/(51 \pm 20)$ nm^2, which is nearly $1e$ per four chains (based on the measured copolymer adsorbance; see the next section). This suggests that some of the free counterions are outside the brush, leaving a net charge at the outer brush surface.[21] Note that the value of κ^{-1} does not depend on the position of the OHP. The high value of ψ compared to that following the STAI coating (essentially uncharged or weakly charged surfaces; see Figure S3) is attributed to the attachment of the charged PMMA-*b*-PSGMA chains onto the STAI-coated mica surfaces. At a separation of less than $D \approx 20 \pm 3$ nm, the force profiles begin to deviate systematically from the DLVO expression (eq 1), displaying a stronger repulsion. This is related to the separation, at which significant overlap between the polymer layers has occurred, so that steric repulsion exceeds the double-layer one. To evaluate the equilibrium thickness L we need to estimate the extent of interpenetration required to exceed the scatter $\Delta F_n \sim 0.5$ mN/m, in the $F_n(D)$ profiles in Figure 1. A comparison with neutral brushes of comparable sizes[66,81] or similar charged polyelectrolyte brushes at high salt concentration[29] suggests that $F_n(D) > 0.5$ mN/m after the two layers have been compressed by 6 ± 1 nm or more from their initial contact, suggesting that in our case $2L = 26 \pm 4$ nm.

In Figure 1, the filled symbols indicate the forces measured upon compression of the polymer layers and open symbols indicate the forces on subsequent decompression. A single compression−decompression cycle took about 10 min. Within

(77) Derjaguin, B. V.; Landau, L. *JETP (USSR)* **1945**, 15.
(78) Verwey, E. J. W.; Overbeek, J. T. G. *Theory of Stability of Lyophobic Colloids*; Elsevier: Amsterdam, 1948.
(79) Claesson, P. M.; Ninham, B. W. *Langmuir* **1992**, *8*, 1406–1412.
(80) Netz, R. R. *Eur. Phys. J. E* **2000**, *3*, 131–141.
(81) Taunton, H. J.; Toprakcioglu, C.; Fetters, L. J.; Klein, J. *Macromolecules* **1990**, *23*, 571–580.
(82) Israelachvili, J. N. *J. Colloid Interface Sci.* **1973**, *44*, 259–272.
(83) Janik, J.; Tadmor, R.; Klein, J. *Langmuir* **1997**, *13*, 4466–4473.
(84) Pashley, R. M.; Israelachvili, J. N. *Colloids Surf.* **1981**, *2*, 169–187.

Table 2. Compression Ratios (β), Shear Forces (F_s), Effective Friction Coefficients (μ_{eff}), and Shear Stresses (σ_s) across the Polyelectrolyte Brushes

D [nm]	$\beta \equiv D/2L$	F_s [nN]	$\mu_{eff} \equiv F_s(D)/F_n(D)$	$\sigma_s \equiv F_s(D)/A_{eff}$ [Nm^{-2}]
5.8	≈4.5	200 ± 30	(5 ± 1) × 10^{-3}	1000 ± 150
7.6	≈3.4	130 ± 30	(3 ± 1) × 10^{-3}	650 ± 150
11	≈2.4	≤30	≤(6 ± 1) × 10^{-4}	≤150

the scatter, no measurable difference in the interaction was observed between compression and decompression profiles. Forces measured on second and third compression−decompression cycles were identical (within the scatter) to those measured in the first cycle, indicating that the polymer chains were not removed by compression or decompression. Normal forces measured during shear (cross symbols) were similar to those measured before shear. $F_n(D)$ profiles measured following shear, on compression (solid circles), were similar to those measured before shear down to $D = 12 \pm 2$ nm (see later).

The surfaces were then separated and enabled to approach slowly from large separations, $D > 10$ nm, under thermal drift (this varies slightly but was typically 0.03 nm/s, for $D > 200$ nm and slower at higher compression). The upper mica surface was made to move laterally back and forth parallel to the lower one at velocity v_s (trace A in Figure 2A). The shear forces F_s transmitted across the polymer layers were simultaneously recorded as the surfaces approached under slow thermal drift. The recorder traces (B, G, and left inset) suggest that no shear forces greater than the noise-limited sensitivity can be observed down to $D = D_j^P$, in the range 6−8 nm, where the surfaces jump into a flat strongly adhesive contact at $D = D_0^P$, in the range 2−3 nm. During the jump itself, as seen in the magnified region of trace G, the magnitude of F_s remains within the apparent noise-level right up to the point C at which the surfaces come into adhesive coupling. Within the scatter this behavior is reproducible on subsequent separations and approaches (traces B and G).

To determine the noise level sensitivity and the magnitude of F_s at D values close to D_j^P, a more careful frequency analysis of the shear traces was performed. The inset shows the frequency (ν) dependence $F_s(\nu)$ of the shear force response, with the arrow showing the drive frequency of the upper mica surface. At this drive frequency, the magnitude of F_s at $D = 11$ nm is within the noise level δF_s (±20−30 nN) of its magnitude at larger separations (e.g., at $D = 35.9$ nm shown in the right inset to Figure 2A). In other words, the resistance to sliding at $D = 11$ is extremely weak and within the sensitivity of the SFB is indistinguishable from its value when the surfaces are far apart. However, the frequency analysis of the shear traces shows that at $D = 7.6 \pm 0.3$ nm $\approx D_j^P$ there is a small (130 ± 30 nN) increase in the amplitude of $F_s(\nu)$ at the frequency, ν, of the back and forth motion applied to the top surface, above its magnitude at large separation. A slightly higher value (200 ± 30 nN) was obtained on the second approach at $D = 5.8 \pm 0.3$ nm.

The value of D_0^P obtained following the jump-in (induced by the shearing motion and compression to ca. 4 mN/m) was significantly smaller than the closest approach distance attainable on normal compression alone (which leads to $D = 10 \pm 1$ nm under a load of ca. 5 ± 1 mN/m). This approach close to contact between the STAI layers is an indication that at the highest compression a significant amount of polymer has been removed from the contact zone by the shear. This shows that the anchoring of the copolymer on the hydrophobized mica by its hydrophobic block is insufficient to prevent the polymer from being sheared off the surfaces at the highest compressions. As $D_0^P < D_0^{STAI}$ and at D_0^P the surfaces are not rigidly coupled (see below), we

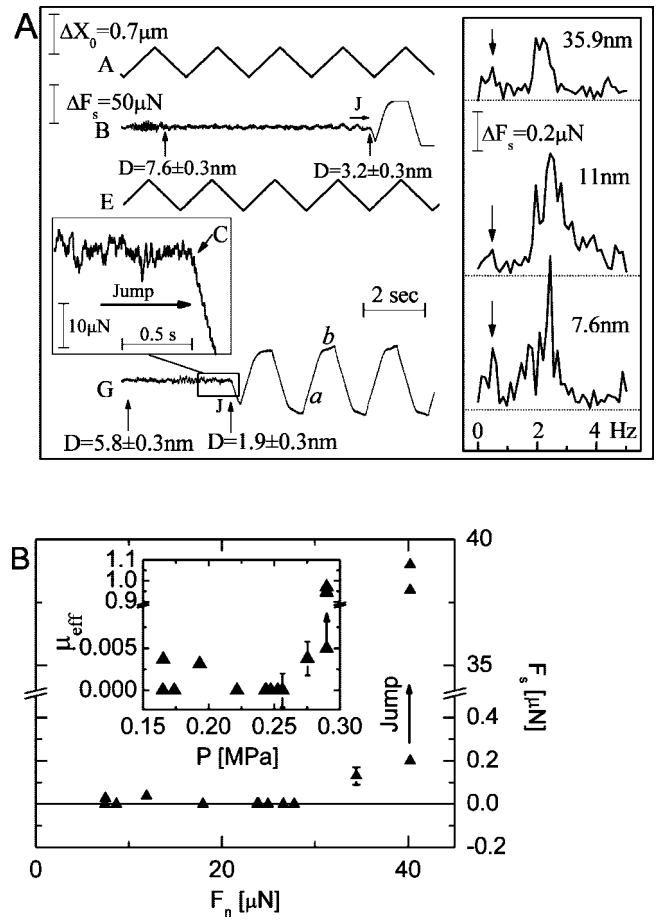

Figure 2. Shear forces between STAI-coated mica surfaces bearing the end-attached PMMA-*b*-PSGMA layers in conductivity water, as the surfaces slide past each other. Trace A (and E) shows the lateral back and forth lateral motion applied to the top mica surface as the surfaces drift slowly towards each other on first (and second) approach. Trace B (and G) shows the corresponding shear force F_s transmitted between the surfaces: it is indistinguishable from the noise until they have jumped together from $D = D_j^P$ in the range 6−8 nm, into a flat adhesive contact at $D = D_0^P$ in the range 2−3 nm (arrow and point C on the expanded left inset), following which the two surfaces are adhesively coupled and slide only slightly past each other as the top surface is made to move laterally (see the text). Frequency analysis (right inset) reveals that the magnitude of F_s at the frequency of the lateral drive motion (0.5 Hz, indicated by arrows) for a surface separation $D = 11$ nm is essentially identical, within the noise-limiting sensitivity ($\delta F_s = \pm 30$ nN) to its value at large separations ($D = 35.9$ nm). Other values are summarized in Table 2. (B) Variation of the shear forces F_s between STAI-coated mica surfaces bearing the end-attached PMMA-*b*-PSGMA layers in conductivity water versus the normal forces F_n. The inset shows the corresponding effective friction coefficient $\mu_{eff} \equiv F_s/F_n$ versus the normal pressure P.

conclude that some of the polymers still remained in the gap. The spontaneous inward motion, which occurs in a single monotonic jump from D_j^P to D_0^P, is driven by the removal of polymers and the consequent resulting imbalance in normal pressure, as well as by the hydrophobic attraction between the STAI-coated surfaces (its duration is estimated at ca. 0.5−1 s). The polymer is probably removed in a rapid cascade of events: above some critical shear stress the first few chains are removed; following this, the shear stress per chain is at least equal to its critical value (before removal of the first chains); thus. more chains are removed, and this process accelerates at D_j^P leading to the jump into D_0^P.

At the adhesive contact (after the jump-in), direct measurement of the flattened area A from the fringe shape gives $A = (1.1 \pm$

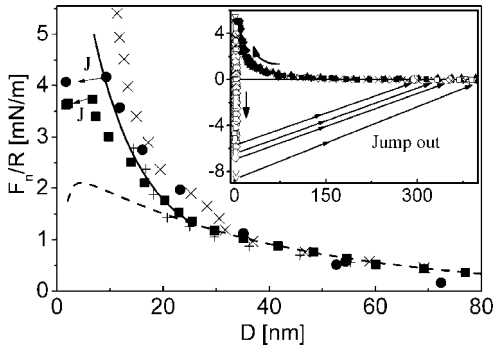

Figure 3. Normalized $F_n(D)$ profiles, measured on compression, during (solid circles) and following (solid squares) shear measurements between STAI-coated mica surfaces bearing the attached PMMA-*b*-PSGMA. The forces are repulsive down to $D = D_j^P$, in the range 6−9 nm, at which point the surfaces jump together into a flat adhesive contact at $D = D_0^P$, in the range 2−3 nm (the jumps are indicated with J and arrows). The broken and solid curves are taken from the corresponding broken and solid curves in Figure 1. For comparison, normal force profiles, before shear, are presented as cross symbols (taken from the profiles in Figure 1). In the inset, we show the $F_n(D)$ profiles over a wider range of data: solid symbols indicate forces measured during compression, open symbols indicate forces measured during decompression, and cross symbols indicate the presheared $F_n(D)$ profiles. The arrows indicate the separation to which the surfaces jump out on pull-off.

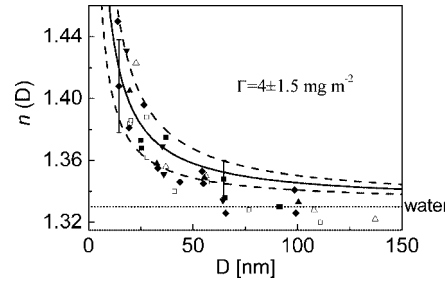

Figure 4. Refractive index $n(D)$ as a function of separation D between curved STAI-coated mica sheets following incubation to saturation in 100 ± 10 μg/mL PMMA-*b*-PSGMA aqueous solution. Results shown are from two different sets of experiments, taken at different contact positions before (solid symbols) or ca. 30 min after (open symbols) shear measurements. The solid curve is the refractive index predicted for $\Gamma = 4$ mg m^{-2} and $n_p = 1.49$ (see the text). The broken curves are the refractive index predicted for $\Gamma = 2.5$ mg m^{-2} (lower curve) and $\Gamma = 5.5$ mg m^{-2} (upper curve), showing that most of the experimental data is within this range. The dotted line indicates the refractive index of water $n_w = 1.333$.

0.3) × 10^{-9} m^2. The traces at D_0^P indicate that the surfaces are moving largely in tandem, though they are not rigidly coupled as was observed after the jump-in to contact between the STAI layers. In general, the applied lateral motion, Δx_0, is related to the sliding between the surfaces, of extent $\Delta x_{sliding}$, and to the bending of the shear spring, of extent Δx, as $\Delta x_0 = \Delta x_{sliding} + \Delta x$. (we recall that the traces show $F_s = k_s \Delta x$). In the first rise regions (regions *a* in the traces), $\Delta x_{sliding}$ represents the extent to which the opposing polymer layers slide past or disentangle from each other as the top surface rubs past the lower one. After the jump at the first cycle, the extent of sliding in region *a* is 25% of Δx_0; then on subsequent cycles it decreases to 18 ± 4% of Δx_0. The extent of sliding increases to 89 ± 2% at the much slower second rise region (region *b* in the traces). This suggests that after the jump the shearing motion has removed a few more polymer chains on the first cycle and allowed stronger adhesion between the STAI layers. On second approach the surfaces jumped into $D_0^P = 1.9 \pm 0.3$ nm instead of $D_0^P = 3.2 \pm 0.3$ nm on first approach, probably because more polymer has been removed on the second approach. In Figure 2B the variation of the shear forces and the effective friction coefficient with the normal load, based on traces such as in Figure 2A and the frequency analysis, are shown.

At the end of each of the shear runs the surfaces were taken apart. At D_0^P the surfaces were strongly adhered and jumped out on separation to D values in the range 300−400 nm. $F_n(D)$ profiles taken immediately (ca. 10 min) subsequent to the shear runs reveal the state of the polymer layers and are shown in Figure 3. Within the scatter, the $F_n(D)$ profiles measured on compression during and after shear resemble their form prior to shear for $D > 12 \pm 2$ nm. At smaller separations the profiles are very different from their preshear forms: instead of strong reversible repulsion they show a jump-in (at $D \sim 8 \pm 2$ nm) on approach of the surfaces and a marked attraction on separating the surfaces following compression, when jump-outs occur, as shown in the inset. The magnitude of the attraction is significantly smaller than that between the STAI-coated surfaces in polymer-free water, suggesting some polymer was trapped between the surfaces, a suggestion borne out by the larger contact separation. Comparison of the before-shear and after-shear $F_n(D)$ profiles shows that some of the polymer chains have been removed from between the surfaces by the shear and the layer has healed partially, but not completely, within ca. 10 min after the shear, though after ca. 30 min the layer recovered (see below).

Refractive Index Measurements. The optical technique used in these experiments also permits the mean refractive index $n(D)$ of the medium between the surfaces to be measured.[82,83] The refractive index of conductivity water at 23 °C, n_w (=1.333), may be compared with $n(D)$ following coverage of the surface by the polymer, and an estimate of the surface coverage can then be made from the increase in the refractive index, at smaller separations. Refractive index profiles are shown in Figure 4 following the attachment of PMMA-*b*-PSGMA to the STAI-coated surfaces. No significant change was observed, within the scatter, during the course of each experiment, either before or ca. 30 min after shear and/or normal force measurements. The error bar in Figure 4 indicates the typical experimental error of a single measurement. The error is relatively larger particularly at the smaller separations; bearing this in mind, we proceed as follows.

The refractive indices measured result from refraction by both the STAI and the solvated polymer layer. We could not measure the refractive index of the STAI layer as it is a very thin layer and the experimental error at small separation is large. We may estimate the surface coverage of STAI on the mica surface, Γ_{STAI}, from the fact that the STAI layer has neutralized nearly all the lattice sites on the mica surface (see Figure S3 of the Supporting Information). Thus, there is one STAI molecule per ca. 0.5 nm^2 (or 2 × 10^{18} STAI molecules/m^2), which is in agreement with an earlier study[68] and in line with the $(CH_3)_3N^+$ headgroup area (0.45 nm^2 [84]). Therefore, $\Gamma_{STAI} = 1$ mg/m^2 (the molecular weight of the STAI is 312 g/mol). As this coverage corresponds to the neutralization of all the ionizable mica lattice sites, this is probably the upper limit on Γ_{STAI}. Assuming uniform distribution of the polymer segments in the gap, the monomer volume fraction ϕ in a gap D is given by

$$\phi = 2\pi/\rho D \tag{2}$$

where Γ is the total surface coverage and ρ is the polymer bulk density (ca. 1 g/cm^3). We also assume that $n(D)$ varies linearly with ϕ as

$$n(D) = n_w + \phi(n_P - n_w) \tag{3}$$

where n_P is the effective refractive index of the polymer layer

and the STAI layer. On the basis of the $n(D)$ data, Γ was evaluated as 4.0 ± 1.5 mg/m^2 assuming n_p as 1.49. The value of n_p is assumed to be close to the refractive index (at 20 °C) of PMMA (1.488), whose backbone resembles that of the PSGMA moiety. This value is also close to the refractive index of a very similar diblock: poly(*tert*-butyl methacrylate)-*b*-PSGMA of comparable molecular weight[3] (assuming the refractive index is proportional to the solution concentration). From this we subtract Γ_{STAI} and obtain the surface coverage of the polymers $\Gamma_p = 3 \pm 1.5$ mg/m^2. The invariance of the surface coverage with D is supported by the refractive index data (Figure 4) and the reversible normal force profiles (Figure 1). The mean spacing s between the attachment points of the polymer on the STAI-coated mica surface is given by

$$s = (M_n/\Gamma_P N_{AV})^{1/2} \quad (4)$$

where M_n is the number-averaged molecular weight of the polymer (28 800 g/mol) and N_{AV} is Avogadro's number. Thus, the value of Γ_P calculated from the refractive index data corresponds to $s = 4 \pm 1$ nm.

Discussion

The main new finding of this study is that relatively short polyelectrolyte brushes attached to hydrophobic surfaces via hydrophobic tails, in conductivity water, dramatically modify the frictional forces between compressed sliding surfaces.[42,65,85–91] Up to moderate compressions, there are extremely low frictional forces, reminiscent of that found between highly extended neutral polymer brushes in a good solvent[52–56,59,92] and significantly lower than between short neutral physigrafted polymers of comparable extension and density[66] or neutral adsorbed polymers in a good solvent[50] or indeed *adsorbed* polyelectrolytes[60,61] or a single polyelectrolyte brush against mica surface.[13] At a relatively high load the polyelectrolyte is removed from the contact region by the shear, as revealed by a jump of the surfaces into a flat adhesive contact and a sharp increase in the friction forces. While the frictional forces between the charged brushes are the main focus of the present paper, it is of interest to examine also the normal interactions, in order to gain insight into the brush structure itself.

Brush Thickness and Density. The brush thickness, L, was estimated from the $F_n(D)$ profiles (Figure 1) as 13 ± 2 nm (including the STAI layer). We can try to estimate the size of each block. The thickness of the hydrophobic part of the chain L_h is not much more than the chain contour thickness[17] (i.e., ca. 0.3 nm), since the sticking energy per hydrophobic PMMA segment on the hydrophobized mica is on the order of k_BT (as estimated from the surface energy between the hydrophobized mica surfaces, Figure S3). The thickness of the STAI layer and the hydrophobic tail together is significantly smaller than the scatter in L.

The fraction of charged groups in the polyelectrolyte that are fully neutralized by counterion condensation, predicted by Manning theory,[93] is $1 - (b/l_B) \approx 0.5$, where l_B is the Bjerrum length given by $l_B = e^2/\varepsilon\varepsilon_0 k_B T \approx 0.7$ nm (at room temperature) and b is the average charge spacing in the fully stretched conformation of the chain. Since the polymer is only ca. 70% charged, b is given by $b = a/\varphi = 0.36$ nm (where $a \sim 2.5$ Å is the monomer size). The fraction f of monomers possessing an ionic group is therefore only $f = \varphi\,(b/l_B) = 0.35$. We can now estimate L on the basis of a scaling model.[1] As s is smaller than the chain dimension and f is not very small, we can assume the diblock to be in the regime $L > \zeta$ (which corresponds to most physical situations), where ζ is the distance scale over which a test charge is neutralized, given by[1]

$$\zeta \approx s\left(a/\pi l_B f^{4/2}\right)^{1/2} = 0.8 \pm 0.1 \text{ nm} \quad (5)$$

and L is then given by[1,17]

$$L \approx f^{4/2} N a \quad (6)$$

For $N = N_2$ (see Table 1) we obtain that $L \approx 17$ nm, close to the experimental value 13 ± 2 nm (bearing in mind also that a prefactor of order unity is missing). The latter is the value we consider for the rest of this discussion

As no salt was added, the expression for L (eq 6) is independent of s and represents the brush thickness when it is highly stretched. L is ca. 45% of the chain contour length. The end to end distance, R_0, of the polyelectrolyte chain is $R_0 \approx (\sqrt{C_\infty}) a N_2^{1/2} = 8.5$ nm (assuming a typical value of 10 for C_∞). The Flory radius, R_F (under good solvent conditions), is larger by a factor of $\sim(N_2/10)^{1/10}$; thus, $R_F \approx 10.8$ nm. The last expression applies for a freely jointed N_2-mer chain, and when steric factors are taken into account, the real Flory radius would be larger. In any case, $R_F > s$ and therefore the polyelectrolyte layers are in a brush-like or a stretched conformation rather than in a nonoverlapping or mushroom regime. The extent of chain stretching and the ratio $L/s = 3.25$ is somewhat lower than that observed with highly extended, high molecular weight neutral brushes[53,81] and higher compared to short neutral brushes with comparable grafting density and Flory radius.[66] Scattering studies[4] indeed show that, in pure water, polyelectrolyte brushes even at low grafting density are more extended than the equivalent neutral brushes.

The mean spacing s between adjacent chains can also be theoretically estimated by minimizing the free energy of the system.[17] It is given by $s \approx a N_1^{1/3} (12\pi k_B T f N_2/A_H)^{1/6} = 3.5$ nm, where $A_H = 1.5 \times 10^{-20}$ J (see the caption of Figure S3), and is in good agreement with the value $s = 4 \pm 1$ nm evaluated from the refractive index measurements. It is important to bear in mind that the expressions used in all cases lack prefactors of order unity so that any close agreements may to some extent be fortuitous. The interactions between the hydrophobic block of the chain and the STAI layer is taken into account as a van der Waals-like interaction rather than a hydrophobic one. The effective value of A_H may then be slightly different, though this should have little effect (ca. 10−20%) on the final result. The dimension of a is likely larger, due to the relatively large side groups along the backbone. The semiquantitative consistency remains however quite clear.

Normal Forces between the Compressed Brushes. As we have $\kappa_s\zeta \cong 0.02 \ll 1$, in the range $D \geq 2L$, the normal forces are expected[1] to decay exponentially with D, as was observed (see Figure 1). The Debye decay length of the long-ranged double-layer repulsive interaction corresponds to an effective ion concentration of $c_s = (5 \pm 1) \times 10^{-5}$ M. This is somewhat lower (by a factor of 2) than the expected value of the effective total free counterion concentration: $N_s c_p f + c_w = (1.1 \pm 0.4) \times 10^{-4}$ M. c_w is the effective ion concentration in conductivity water and in a dilute solution of PMMA-*b*-PSGMA (see the Supporting

(85) Briscoe, W. H.; Titmuss, S.; Tiberg, F.; Thomas, R. K.; McGillivray, D. J.; Klein, J. *Nature* **2006**, *444*, 191–194.
(86) Klein, J.; Perkin, S.; Kampf, N. *Abstr. Papers Am. Chem. Soc.* **2006**, 231.
(87) Perkin, S.; Chai, L.; Kampf, N.; Raviv, U.; Briscoe, W.; Dunlop, I.; Titmuss, S.; Seo, M.; Kumacheva, E.; Klein, J. *Langmuir* **2006**, *22*, 6142–6152.
(88) Perkin, S.; Kampf, N.; Klein, J. *Phys. Rev. Lett.* **2006**, 96.
(89) Briscoe, W. H.; Klein, J. *J. Adhes.* **2007**, *83*, 705–722.
(90) Tsarkova, L.; Zhang, X.; Hadjichristidis, N.; Klein, J. *Macromolecules* **2007**, *40*, 2539–2547.
(91) Klein, J. *Phys. Rev. Lett.* **2007**, 98.
(92) Klein, J. *Colloids Surf. A* **1994**, *86*, 63–76.
(93) Manning, G. S. *J. Chem. Phys.* **1969**, *51*, 924–933.

Information). c_p is the polymer concentration. We attribute the main reason for this discrepancy to the fact that in the solution most of the chains are isolated from each other and there is little overlap between their associated counterions.[94] Inside the brush, the average concentration of free counterions is $c_{in} \approx fN_2/N_{AV}Ls^2 = 0.32$ M. Most of these counterions are inside the brush and do not contribute to the long-ranged normal forces. The small fraction that extends beyond the outer brush surface provides an effective net surface charge and thereby contributes (together with the free counterions in the solution) to the observed long-ranged osmotic pressure in the gap.[1]

c_{in} is significantly greater than the external ion concentration in solution; thus, chain stretching results from the osmotic pressure of the confined counterions when compressed to separation D smaller than $2L$,[1] $\Pi_{osm} \approx 2fN_2k_BT/Ds^2$. This osmotic pressure is resisted by the elastic force of the chain, which corresponds to a pressure of $\Pi_{el} \approx kD/s^2$, where k is the elastic constant given by $k \approx k_BT/N_2a^2$. The total osmotic pressure in the range $D < 2L$ is therefore $\Pi = \Pi_{el} - \Pi_{osm}$. The contribution of this to the normal force may be estimated by integrating the osmotic pressure from $2L$ to D

$$F_n(D)/R \approx 2\pi \int_{2L}^{D} \Pi(D')\, dD' \approx 2\pi k_BT/s^2[(2L)^2/N_2a^2((D/2L)^2-1) - 2fN_2 \ln(2L/D)] \quad (7)$$

Using eq 6 we obtain

$$F_n(D)/R \approx 4\pi k_BTfN_2s^{-2}[2((D/2L)^2 - 1) - \ln(2L/D)] \quad (8)$$

The total normal force in the range $D < 2L$ is then given by the sum[95] of the DLVO expression (eq 1) at $D = 2L$ (using the parameters of the long-ranged interaction) and $F_n(D)$:

$$F_n(D)/R \approx 4\pi k_BT\{fN_2s^{-2}[B((D/2L)^2 - 1) - A \ln(2L/D)] + 32c\kappa^{-1} \tanh^2(e\psi_0/4k_BT) \exp(-2\kappa L)\} - [A_H/6D^2] \quad (9)$$

where A and B are prefactors to account for the unknown prefactors in the elastic and osmotic pressure terms.[96] The agreement of eq 9 with the data (see Figures 1 and 3) is reasonable, bearing our approximations in mind, particularly for compression ratios $\beta \equiv 2L/D < 3$. The ratio $A/B \approx 3$ found (see Figure 1) suggests that the osmotic repulsion dominates the elastic force. It can be shown[1] that the repulsive forces between polyelectrolyte brushes are stronger than that between neutral polymer brushes of the same brush thickness and grafting density. This is due to the additional repulsive contribution of the osmotic pressure of the counterions inside the polyelectrolyte brush.

Shear Forces. The shear forces between the compressed brushes are below our detection limit (±20−30 nN) down to separation distance $D = 11$ nm (see Figure 2A) within the range of shear velocities, v_s, used (220−550 nm/s). Very weak shear forces (130 ± 30 nN) are first measured close to D_j^P (e.g., at $D = 7.6$ nm, Figure 2A, trace B) just before the surfaces jump into D_0^P, after which they are strongly coupled and move largely in tandem. We may define an effective friction coefficient $\mu_{eff} \equiv F_s(D)/F_n(D)$. If we consider the magnitude of $F_n(D)$ just before the onset of measurable $F_s(D)$ to be its value from the $F_n(D)$ profiles and the magnitude of F_s at that point to be $\delta Fs \leq 30$ nN, we obtain that $\mu_{eff} \leq (6 \pm 1) \times 10^{-4}$ at $D = 11$ nm. It is of interest to evaluate the effective corresponding local pressures. The effective contact area A_{eff} is given by the Hertzian contact mechanics expression,[97] and $A_{eff} = \pi(RF_n/K)^{2/3} = (2 \pm 1) \times 10^{-10}$ m^2, where $K = (1 \pm 0.3) \times 10^9$ N/m^2.[34] We thus obtain that the mean pressure over the contact area is given by $P \approx F_n(D)/A_{eff} = (2.5 \pm 1) \times 10^5$ N m^{-2} $\approx 2.5 \pm 1$ atm (The total number of chains in the contact area is $A_{eff}/s^2 = (8 \pm 4) \times 10^7$). The shear stress is given by $\sigma_s \equiv F_s(D)/A_{eff}$. At $D = 11$ nm, $\sigma_s \leq 150$ N m^{-2}. Other values are summarized in Table 2. The increase in the shear stress with decreasing D may originate in an increase of the effective viscosity, resulting from the increase in the monomer volume fraction as the separation decreases (see eq 2). We note that, although the relative shear velocity, v_s, of the surfaces is known, the actual shear rate, v_s/d, over the interpenetration zone of width d, is less straightforward to evaluate, since d, while certainly much smaller than D, is not easy to estimate (see the Appendix) and in any case may change with v_s itself.[59]

At low and moderate compression, i.e., $D > 2L$, the load is balanced by the osmotic pressure of counterions in the gap between the brushes. The virtual absence of frictional drag at $D > 2L$ is attributed to the presence of a fluid water layer that separates the nonoverlapped opposing chains.[37,38] The reason for the low frictional forces at higher compression (and overlap) is related in part to the small interpenetration distance d between the compressed polyelectrolyte brushes (see the Appendix). The weak interpenetration of opposite chains, resulting in minimal entanglement at the interface, even when the brushes are strongly compressed, is what—in line with the results for neutral brushes—ultimately leads to the very low effective friction coefficients. At the same time, each of the charged segments rubbing against others within the sheared interpenetration zone is surrounded by a hydration sheath. As has recently been demonstrated,[38] such sheaths are tenaciously bound to the charges but are at the same time very fluid and so serve as efficient lubricating layers. Detailed comparison between this system and other types of polymeric surfactant[61] show that polyelectrolyte brushes are able to reduce friction efficiently, even when compressed to volume fraction close to unity, while other types of polymeric surfactants (adsorbed polyelectrolytes and neutral brushes in nonpolar and aqueous media) result in significant frictional forces at volume fractions larger than 0.2−0.3. This suggests that while the viscosity of the polyelectrolyte chains at a concentration corresponding to that in the compressed brush layers may be very high, nonetheless the interface between the two charged brushes is highly fluid. This is attributed primarily to the weak segmental interpenetration together with the (shear) fluidity of compressed hydrated layers.

(94) The polyelectrolyte concentration is $(3.5 \pm 0.3) \times 10^{-6}$, and each chain has 80 ions; thus, the total ion concentration is on the order of 10^{-4}. The polyelectrolyte localizes the ions in its vicinity and at this concentration the chains are about 100 nm apart, whereas their size is only a few nanometers and their neutralization length is less then 1 nm (see the Discussion). Thus, counterions associated with different chains do not overlap. In addition, the chains essentially do not adsorb onto the mica surfaces and are not expected to remain in the gap. We therefore conclude that the contribution of the nonadsorbing polyelectrolytes to the screening length in this case is very small. Recently, a quantitative treatment of this case was reported by Tadmor et al. (*Macromolecules* **2002**, *35*, 2380). Within the scatter, our data is in agreement with this treatment.

(95) We note that by assuming this additivity we may double count at $D < 2L$ the contribution of the small fraction of counterions that are outside the brush. However, this should have a negligible effect.

(96) The magnitudes of A and B (Figure 5 caption) are, at ca. 10^{-2}, significantly smaller than expected from a scaling treatment as we have here. The reason may be that using N_2 in the expression for the elastic constant, k, in our treatment implies ideal freely jointed chains. In reality, the number of equivalent freely jointed segments must be significantly smaller then the number of monomers N_2, and this could correspondingly lead to larger and more reasonable (order unity) A and B values.

(97) Johnson, K. L.; Kendall, K.; Roberts, A. D. *Proc. R. Soc. (London), Ser. A* **1971**, *324*, 301–313.

(98) Moro, T.; Takatori, Y.; Ishihara, K.; Konno, T.; Takigawa, Y.; Matsushita, T.; Chung, U.; Nakamura, K.; Kawaguchi, H. *Nat. Matter* **2004**, *3*, 829–836.

(99) Zhulina, E. B.; Borisov, O. V.; Birshtein, T. M. *J. Phys. II* **1992**, *2*, 63–74.

(100) de Gennes, P. G. *Scaling Concepts in Polymer Physics*; Cornell Univ. Press: Ithaca, NY, 1979.

We may also estimate an upper limit to the amount of polymer retained in the gap following shear, from the value of D_0^P. On first approach during shear $D_0^P = 3.0 \pm 0.5$ nm, whereas on second approach $D_0^P = 2.1 \pm 0.5$ nm. Subtracting ca. 1 nm for the STAI layers and assuming a bulk polymer density of ca. 1 g/cm^3, we find that on first compression during shear the amount of polymer Γ that remains on each STAI layer is less than ca. 1 mg/m^2 $\approx 0.3\Gamma_p$, whereas on second compression $\Gamma \leq$ ca. 0.5 mg/m^2 $\approx 0.15\Gamma_p$, where Γ_p is the unperturbed polymer surface coverage. The variation in the adhesion energy following shear (as deduced from the pull-off force) correlates with the value of Γ: it is higher for lower Γ as more STAI molecules are exposed to the water phase.

The "healing" properties of the polyelectrolyte brushes are of interest. The refractive index measurements (Figure 4) suggest that chains that have been removed by the shear reattached within 30 min, similar to behavior observed with neutral brushes.[54] Moreover, $F_n(D)$ profiles measured ca. 10 min following shear (Figure 3) exhibit similar repulsive force to that measured before shear for $D > 12 \pm 2$ nm, suggesting that significant recovery of the polymer layers has occurred already over this time scale. This is in line with an earlier adsorption kinetics study of a very similar diblock copolymer on a hydrophobic surface.[3]

Finally, we note that preliminary results with added salt (to concentration ca. 10^{-2} M) show that more chains are attached on the STAI layers and the range of electrostatic normal interaction decreases as expected and also as measured in a similar system.[29] Importantly, the short-ranged normal interactions are steeper and stronger due to the additional polymer absorbance, but as our preliminary measurements show, the frictional forces even at higher salt concentrations (ca. 10^{-2} M NaCl) remain extremely weak, as in pure water, resulting in $\mu_{eff} \sim 10^{-4}$, up to comparably high pressures. We also found that about 20% longer hydrophobic block is sufficient to prevent chain removal upon shear, in the shear rates applied in this study.

Summary and Conclusions

Block copolymers with one hydrophobic block that adsorbs on hydrophobized mica surfaces and with polyelectrolyte as the other block were used to form polyelectrolyte brushes each of thickness L ($L = 13 \pm 2$ nm). Long-range electrostatic repulsive forces between the polymer-bearing surfaces were detected already at $D > 2L$ due to the osmotic pressure of the free counterions outside the brushes, whereas at smaller separations ($D < 2L$) the repulsive forces are dominated by the interaction between the brushes themselves. While normal forces between polyelectrolyte−brush layers have been earlier reported,[6,29] our most striking new finding concerns the massive reduction in frictional forces by such brushes. We attribute the weakness of the frictional forces in part to factors similar to those acting in the case of lubrication by neutral brushes in good solvents,,[52] that is, weak interpenetration of the mutually compressed brushes when under high loads (and therefore a fluid interfacial region under shear). In addition, however, and in contrast to neutral brushes, in the case of polyelectrolytes the resistance to interpenetration arising from polymer configurational entropy is augmented by the osmotic pressure of counterions trapped in the brush layers. At the same time, highly fluid hydration sheaths are strongly bound to the charged segments and serve as lubricating layers, much as hydrated monovalent ions do. The charged brushes are currently the most effective type of polymeric surfactants[61] in reducing the effective friction coefficient, μ_{eff}, which in our studies attains values as low as $\mu_{eff} \sim (5 \times 10^{-3})-(5 \times 10^{-4})$, at pressures up to a few atmospheres. The particular interest in this is that such pressures are relevant to those in living systems, where interfacial sliding is believed to be mediated by polyelectrolytes at the surfaces.[61−63,65] In this context of lubrication, we note also that even when the polyelectrolyte brushes are eventually detached from the surfaces during sliding, at the highest loads, they recover by healing over a time scale of tens of minutes.

Finally we note that in our brief report on lubrication by polyelectrolyte brushes[61] we explicitly remarked that our findings could be applied to "the design of lubricated surfaces in artificial implants". It is thus of particular interest that, barely a year later, precisely this idea of coating by charged brushes was applied to the polymeric surface of a hip prostheses, and indeed resulted in a reduction of friction, and in particular in a very considerable reduction in the wear.[98]

Acknowledgment. We thank Xueyan Zhang for help in preliminary experiments, Joseph Frey for synthesis of the STAI surfactant, Rafael Tadmor for advice, and Tom Witten, Philip Pincus Anton Zilman, Sam Safran, Dima Lukatsky, and Oleg Borisov for useful discussions and correspondence. We also thank the Eshkol Foundation for a studentship to U.R., the Canadian Friends of the Weizmann Institute for a Charpak-Vered Exchange Fellowship (S.G.), and the Israel Science Foundation, the McCutchen Foundation, the Deutsche-Israelische Program (DIP), and the Minerva Foundation at the Weizmann institute for their support of this work.

Appendix. Estimating the Interpenetration of Polyelectrolyte Brushes

To estimate the interpenetration distance d between two polyelectrolyte brush layers, we consider the penetration of one chain into the field of the opposing layer, similar to the treatment of neutral brushes.[53] Let $\mu(z)$ be the potential per monomer at distance z from the surface. We are assuming a Gaussian density profile of the monomers in the charged polymer brush[99] and that $\mu(z)$ is proportional to the density profile. Thus $\mu(z) \approx \alpha(Na^3/Ls^2) \exp(-z^2/L^2) = \mu(0) \exp(-z^2/L^2)$, where L is the thickness of the layer, α is the proportionality constant, and s is the spacing between grafted chains. If there are n_m monomers that penetrate the opposite layer, then for a random coil

$$d^2 = n_m a^2 = (n_m/N)R^2 \tag{A1}$$

where $R^2_0 = Na^2$. The mean potential per monomer of the moiety located between $z = L$ and $z = L - d$ is approximated by the potential at $z = L - (d/2)$. For d not too large, this is given by

$$\mu(L - (d/2)) \approx d/2[\partial\mu/\partial z]_{z=L} \approx \alpha(dNa^3/L^2s^2) = \mu(0)d/L \tag{A2}$$

The total energy cost of an n_m-monomer penetration into the opposite layer at equilibrium equals the random thermal energy and is given by

$$n_m\mu(L - (d/2)) \approx k_BT \tag{A3}$$

where $L \approx D/2$, and D is the distance between the two surfaces. The energy cost for the penetration of all the chain is dominated by the random coil elastic stretching energy,[100] $(L/R_0)^2k_BT$. $\mu(0)$ is given by the potential of a fully stretched N-mer in the brush; thus, we find that

$$N\mu(0) = (L/R_0)^2k_BT \tag{A4}$$

By substituting eq A4 in eq A3 and using the relations A1 and A2, we finally find that

$$d \approx L^{-1/3} R_0^{4/3} \sim D^{-1/3} \quad \text{(A5)}$$

Prefactors (lacking in the scaling relations) could slightly alter this result. This result is equivalent to that obtained for neutral polymer brushes,[53] despite the exponential as opposed to the parabolic form of the potential $\mu(z)$, indicating that the interpenetration zone d between the two layers varies rather weakly with the layer compression. A more realistic model of the polyelectrolyte brushes, taking into account their electrostatic repulsion and excluded volume effects,[18] may well yield an even weaker interpenetration.

Glossary

γ_w	solid−liquid surface tension in conductivity water
γ_s	surface tension between STAI layers in conductivity water
Γ	the total surface coverage
Γ_{STAI}	surface coverage of STAI
Γ_p	surface coverage of the polymers
κ^{-1}	Debye decay length
κ_w^{-1}	Debye decay length measured between bare mica surface in conductivity water and in dilute solution of PMMA-*b*-PSGMA
κ_s^{-1}	Debye decay length measured after addition of PMMA-*b*-PSGMA to the STAI-coated mica surfaces
Π_{osm}	osmotic pressure of the confined counterions
Π_{el}	elastic pressure
Π	total osmotic pressure
σ_0	effective (large separation) surface charge
σ_s	shear stress
φ	degree of sulfonation
ϕ	the monomer volume fraction
A	contact area
A_{eff}	effective contact area
A_H	Hamaker constant
c	ion concentration
c_w	effective ion concentration in conductivity water and in dilute solution of PMMA-*b*-PSGMA
c_s	effective ion concentration after addition of PMMA-*b*-PSGMA to the STAI-coated mica surfaces
c_{in}	the average concentration of free counterions inside the brush
c_p	polymer concentration
d	interpenetration distance between the compressed polyelectrolyte brushes
D_0	zero distance between the mica surfaces in conductivity water
D_0^{STAI}	distance between the STAI-coated mica surfaces at flat contact
D_0^P	distance between the polyelectrolyte brushes at contact, after the jump-in
D_j	jump distance between the mica surfaces in conductivity water
D_j^{STAI}	jump distance between the STAI-coated mica surfaces in conductivity water
D_j^P	jump distance between the polyelectrolyte brushes, during or after shear
D_h	outer Helmholtz plane (OHP)
f	fraction of monomers possesses an ionic group
L_0	the thickness of the dry surfactant layer
L_h	the thickness of the hydrophobic block
L	the equilibrium thickness of the polyelectrolyte brush
n	refractive index
n_w	refractive index of water
n_P	the effective refractive index of the polymer layer and the STAI layer
n_m	number of monomers that penetrate into the opposite layer
N_1	number of monomers in the hydrophobic chain
N_2	number of monomers in the hydrophilic chain
N_s	the number of monomers that contain a sulfonate group

Supporting Information Available: Additional experimental details. This material is available free of charge via the Internet at http://pubs.acs.org.

LA7039724